

Multifunction Phasor Analysis for Distribution Networks

Guglielmo Frigo, Giada Giorgi, Matteo Bertocco and Claudio Narduzzi

Department of Information Engineering

University of Padova, Padova, Italy

frigogug@dei.unipd.it, {giada.giorgi, matteo.bertocco, claudio.narduzzi}@unipd.it

Abstract—To effectively manage the growing number of distributed energy resources, PMU-based monitoring is being investigated for electrical distribution networks. In this context, a very challenging combination of constraints and cost-effectiveness requirements must be taken into account, suggesting the need for new-generation devices. In this paper we discuss performances of a compressive sensing phasor measurement algorithm, based on a Taylor-Fourier multifrequency signal model, as a tool for monitoring and managing smart distribution networks.

I. INTRODUCTION

Power transmission grids are monitored by wide-area measurement systems relying on phasor measurement units (PMUs). To effectively manage the growing number of distributed energy resources, a similar monitoring is envisaged for electrical distribution networks. Extension of the PMU concept is far from straightforward, suggesting the need for new-generation devices. A measuring unit for distribution networks must take into account a very challenging combination of constraints and cost-effectiveness requirements. Because of the shorter length of distribution lines, accurate measurement of very small phase changes is critical to phasor analysis. Furthermore, the reduced scale of aggregation in generation and power demand profiles emphasises, in relative terms, the impact of generation and load variations, as well as the effect of power quality (PQ) impairments.

In this context, devices having the flexibility to operate both as a PMU and as a harmonic phasor and PQ analyzer could provide innovative and cost-effective solutions. The key to the realization of such a unit lies in the flexibility and adaptability of measurement algorithms, supported by a common signal conditioning and data acquisition hardware platform.

A multifrequency dynamic phasor model is well suited to this framework, but dealing with the variety of conditions occurring in practice [1] requires the support of a suitable algorithm. In general, Fourier-based algorithms (e.g., [2], [3]) are well suited to multifrequency analysis. Taylor-Fourier analysis has also been applied to dynamic phasors, in the harmonic case as the Taylor-Fourier transform (TFT) [4], [5]. To deal with the off-nominal issue, TFT has been further refined to include iterative estimation of the actual fundamental frequency [6]. The application of compressive sensing (CS) in the context of phasor measurement was first proposed in [7]. A CS-based algorithm for synchrophasor measurement based on a multifrequency model was discussed and characterized

in [8], showing that accuracy is significantly improved by including in the estimate the few harmonic and/or interharmonic dynamic phasors close to the fundamental frequency.

In this paper we discuss the use of a full Taylor-Fourier multifrequency (TFM) signal model, aiming at the accurate measurement of a whole set of harmonic and interharmonic components. We investigate phasor analysis performances in particularly demanding real-life conditions and show that the approach can be effective for a variety of applications in monitoring and control of smart distribution networks.

II. MULTIFREQUENCY DYNAMIC PHASORS

A power system waveform represented by a sum of sinusoidal components, with time-varying amplitudes and phases, takes the discrete-time form:

$$x[n] = \sum_{f_h \in S_h} A_h[n] \cos(2\pi f_h n T_s + \phi_h[n]) \quad (1)$$

where T_s is the sampling interval and S_h is a generic set of frequencies, that includes the power system frequency f_1 , its harmonic multiples and generic interharmonic frequencies.

The multifrequency dynamic phasor representation of (1) is:

$$x[n] = \frac{1}{\sqrt{2}} \sum_{f_h \in S_h} \bar{\mathbf{X}}_h[n] e^{j2\pi f_h n T_s} + \bar{\mathbf{X}}_h^*[n] e^{-j2\pi f_h n T_s}, \quad (2)$$

where dynamic phasors $\bar{\mathbf{X}}_h[n]$ are defined as:

$$\bar{\mathbf{X}}_h[n] = \frac{A_h[n]}{\sqrt{2}} e^{j\phi_h[n]}, \quad h \in S_h \quad (3)$$

Sample acquisition spans an observation interval T_W , whose mid-point is taken to coincide with the reporting instant in a phasor measurement algorithm. In the following we consider a sequence length of $2N+1$ samples, that is: $T_W = (2N+1)T_s$, within the index range $-N \leq n \leq +N$, so that the phase reference coincides with $n = 0$. Usually, T_W is also assumed to span an integer number M of periods of the nominal power system frequency f_0 , which assures exact estimates for any multiple of frequency (f_0/M).

The CSTFM algorithm [8] considers the approximation of phasor $\bar{\mathbf{X}}_h[n]$ by a K -order Taylor-series expansion, as

proposed in [9]. This yields the TFM model:

$$x[n] = \frac{1}{\sqrt{2}} \sum_{f_h \in S_h} \left[\sum_{k=0}^K \mathbf{p}_{f_h}^{(k)} \frac{(nT_s)^k}{k!} e^{j2\pi f_h n T_s} + \mathbf{p}_{f_h}^{*(k)} \frac{(nT_s)^k}{k!} e^{-j2\pi f_h n T_s} \right]. \quad (4)$$

where the complex Taylor-Fourier (TF) coefficients $\mathbf{p}_h^{(k)}$ are the k -th order derivatives of $\bar{\mathbf{X}}_h(nT_s)$ at $n = 0$.

The contribution to model equation (4) by a single frequency phasor component can be written in different form using the formalism introduced in [6]. We consider ‘‘time’’ vectors:

$$\begin{aligned} \underline{\mathbf{t}}^{(0)} &= [1 \dots 1 \dots 1 \dots 1]^T \\ \underline{\mathbf{t}}^{(1)} &= [(-NT_s) \dots 0 \dots nT_s \dots NT_s]^T \\ &\vdots \\ \underline{\mathbf{t}}^{(K)} &= \left[\frac{(-NT_s)^K}{K!} \dots 0 \dots \frac{(nT_s)^K}{K!} \dots \frac{(NT_s)^K}{K!} \right]^T \end{aligned} \quad (5)$$

and form with them the $(2N + 1) \times (K + 1)$ matrix:

$$\mathbf{T} = [\underline{\mathbf{t}}^{(0)} \underline{\mathbf{t}}^{(1)} \underline{\mathbf{t}}^{(2)} \dots \underline{\mathbf{t}}^{(K)}]. \quad (6)$$

Next, we define a $(2N + 1) \times (2N + 1)$ diagonal matrix of exponential terms at phasor frequency f_h :

$$\mathbf{E}_{f_h} = \frac{1}{\sqrt{2}} \text{diag} [e^{j2\pi f_h n T_s}]_{-N \leq n \leq +N}. \quad (7)$$

noting that, since \mathbf{E}_{f_h} is diagonal, $\mathbf{E}_{f_h}^T = \mathbf{E}_{f_h}$ and $\mathbf{E}_{f_h}^H = \mathbf{E}_{f_h}^*$. The contribution of a single dynamic phasor $\bar{\mathbf{X}}_h[n]$ can be represented by the elements of the matrix-vector product: $\mathbf{E}_{f_h} \mathbf{T} \underline{\mathbf{p}}_{f_h}$, with $\underline{\mathbf{p}}_{f_h} = [\mathbf{p}_{f_h}^{(0)} \dots \mathbf{p}_{f_h}^{(K)}]^T$.

Writing the full TFM model (4) in matrix form requires to introduce the parameter vector:

$$\underline{\mathbf{p}}_{S_h} = [\underline{\mathbf{p}}_{f_1}^T \dots \underline{\mathbf{p}}_{f_h}^T \dots (\underline{\mathbf{p}}_{f_h}^*)^T \dots (\underline{\mathbf{p}}_{f_1}^*)^T]^T \quad (8)$$

and the corresponding matrix:

$$\mathbf{E}_{S_h} = [\mathbf{E}_{f_1} \dots \mathbf{E}_{f_h} \dots \mathbf{E}_{f_h}^* \dots \mathbf{E}_{f_1}^*] \quad (9)$$

that allow to write (4) as:

$$\underline{\mathbf{x}} = \mathbf{E}_{S_h} \begin{bmatrix} \mathbf{T} & 0 & \dots & 0 \\ 0 & \mathbf{T} & & \vdots \\ \vdots & & \ddots & 0 \\ 0 & \dots & 0 & \mathbf{T} \end{bmatrix} \underline{\mathbf{p}}_{S_h} \quad (10)$$

It should be emphasized that all phasor frequencies in the TFM model are unknowns in a continuous range of values.

We preliminarily recall the case of a single dynamic phasor at the nominal power system frequency f_0 . Parameter vector (8) simply becomes: $\underline{\mathbf{p}} = [\underline{\mathbf{p}}_0^T (\underline{\mathbf{p}}_0^*)^T]^T$, and the least-squares estimate is [6]:

$$\hat{\underline{\mathbf{p}}} = \begin{bmatrix} \mathbf{T}^T \mathbf{T} & \mathbf{T}^T (\mathbf{E}_{f_0}^*)^2 \mathbf{T} \\ \mathbf{T}^T (\mathbf{E}_{f_0})^2 \mathbf{T} & \mathbf{T}^T \mathbf{T} \end{bmatrix}^{-1} \begin{bmatrix} \mathbf{T}^T \mathbf{0} \\ \mathbf{0} \mathbf{T}^T \end{bmatrix} \begin{bmatrix} \mathbf{E}_{f_0}^* \\ \mathbf{E}_{f_0} \end{bmatrix} \underline{\mathbf{x}} \quad (11)$$

where the column vector $\underline{\mathbf{x}}$ contains the sample sequence $x[n]$.

The two products: $\mathbf{T}^T \mathbf{E}_{f_0}^* \underline{\mathbf{x}}$ and $\mathbf{T}^T \mathbf{E}_{f_0} \underline{\mathbf{x}}$ can be interpreted either in terms of a filtering operation or by considering *time windows*. The latter viewpoint is better suited to the analysis of a TFM model. Introducing the normalized frequency $\nu = f T_s$, the discrete-time Fourier transform (DTFT) of window $\underline{\mathbf{t}}^{(k)}$ is:

$$T^{(k)}(\nu) = \sum_{n=-N}^{+N} \frac{(nT_s)^k}{k!} e^{-j2\pi \nu n} = \left(\frac{jT_s}{2\pi k!} \right)^k \frac{d^k}{d\nu^k} D(\nu) \quad (12)$$

where $D(\nu)$ is the Dirichlet kernel:

$$D(\nu) = \frac{\sin[\pi \nu (2N + 1)]}{\sin \pi \nu}. \quad (13)$$

When the actual power system frequency f_1 differs from f_0 , a suitable choice of the TF order K allows to preserve accuracy of the fundamental phasor measurement, but spectral leakage caused by the finite-length observation interval is unavoidable. Consequently, at multiples of the frequency step $\Delta_f = 1/T_W$ spurious terms are produced, whose magnitudes can prevent accurate estimation of other phasor components.

At high levels of accuracy, synchrophasor total vector error (TVE) can also be affected significantly by interference from nearby harmonic and interharmonic components. Accuracy improvement in fact motivated consideration of a TFM model in [8] although, in the interest of reduced computational load, the number of additional phasors was kept to a minimum.

III. CSTFM ALGORITHM FOR PHASOR ANALYSIS

Whereas a PMU is concerned with the single most significant component of (2), measurement of harmonic or interharmonic phasors requires specific attention to be paid in ensuring accuracy also at low signal levels. Components of practical interest may be far smaller than the fundamental and, assuming for instance target TVE to be 1% of the fundamental, the error vector could be approximately the same order of magnitude as most harmonic and interharmonic phasors.

Accurate measurement of all dynamic phasors requires determination of frequencies f_h with small uncertainty, to avoid potential mutual interference among phasor component estimates. By the CSTFM algorithm we achieve enhanced frequency accuracy with no increase in measurement time.

Since the set of frequencies S_h is unknown, we start by defining a set of *candidate* frequencies f_l on a uniform frequency grid with a finer step $\Delta'_f = \Delta_f/P$:

$$f_l = l \Delta'_f \quad \text{with: } \Delta'_f = \frac{1}{P T_W}, \quad 0 \leq l \leq PN. \quad (14)$$

Parameter vector size must grow accordingly, thus we consider (using only index l as a subscript henceforward):

$$\underline{\mathbf{p}} = [\underline{\mathbf{p}}_0^T \underline{\mathbf{p}}_1^T \dots \underline{\mathbf{p}}_{PN}^T (\underline{\mathbf{p}}_{PN}^*)^T \dots (\underline{\mathbf{p}}_1^*)^T]^T, \quad (15)$$

whose size is $(K + 1) \times P \times (2N + 1)$. Likewise, we refer to matrix \mathbf{E} , formed by $P \times (2N + 1)$ diagonal blocks \mathbf{E}_l and indicate by $[\text{diag}\{\mathbf{T}\}]$ the block diagonal matrix formed with the same number of equal submatrices \mathbf{T} . This yields:

$$\underline{\mathbf{x}} = \mathbf{E} [\text{diag}\{\mathbf{T}\}] \underline{\mathbf{p}} \quad (16)$$

To show the relation between this equation and the CSTFM formulation in [8], it suffices to define the $(2N+1) \times (2N+1)$ matrix \mathbf{W} whose elements are the complex exponentials: $[\mathbf{W}]_{m,n} = e^{-j[2\pi mn/(2N+1)]}$ and note that the following identity holds:

$$\underline{\mathbf{x}} = \mathbf{W}^H \frac{1}{2N+1} \mathbf{W} \mathbf{E} [\text{diag}\{\mathbf{T}\}] \underline{\mathbf{p}} = \mathbf{W}^H \mathbf{D} \underline{\mathbf{p}}. \quad (17)$$

Hence, the dictionary matrix \mathbf{D} of [8] can be expressed in terms of the quantities considered in the present paper.

We remind that (16) is highly underdetermined. By the CS approach its maximally *sparse* solution, that is, the vector $\hat{\underline{\mathbf{p}}}$ having the least number of non-zero elements is found as:

$$\begin{aligned} \hat{\underline{\mathbf{p}}} &= \arg \min_{\underline{\mathbf{p}}} \|\underline{\mathbf{p}}\|_0 \\ &\text{subject to: } \|\underline{\mathbf{x}} - \mathbf{E} [\text{diag}\{\mathbf{T}\}] \underline{\mathbf{p}}\|_2 \leq \zeta \end{aligned} \quad (18)$$

where the pseudo-norm $\|\underline{\mathbf{p}}\|_0$ indicates the number of non-zero elements of $\underline{\mathbf{p}}$, and ζ is a given threshold.

It should be remarked that higher-order TF coefficients are Taylor-series refinements of the *same* dynamic phasor, therefore a sub-vector $\underline{\mathbf{p}}_l$ must be dealt with as a single unit within $\underline{\mathbf{p}}$. Since solving (18) by the basic Orthogonal Matching Pursuit (OMP) approach [10] would not satisfy this constraint, we adapted it as summarized in the following.

The estimate of $\underline{\mathbf{p}}$ as a sparse vector is obtained by constructing the index set S defined as:

$$S = \left\{ l_h : |l_h \Delta'_f - f_h| < \frac{\Delta'_f}{2}, f_h \in S_h \right\}. \quad (19)$$

By definition, all subvectors $\underline{\mathbf{p}}_l$ for which $l \notin S$ can be set to $\underline{\mathbf{0}}$ in the parameter vector (8). This allows to consider a *restricted* parameter vector $\underline{\mathbf{p}}_S$ and a correspondingly reduced matrix \mathbf{E}_S , where only the relevant columns are retained. The number of blocks in $[\text{diag}\{\mathbf{T}\}]_S$ is also decreased accordingly. The least-squares solution of the resulting equation:

$$\underline{\mathbf{x}} = \mathbf{E}_S [\text{diag}\{\mathbf{T}\}]_S \underline{\mathbf{p}}_S \quad (20)$$

provides the TF coefficients of phasors in the TFM model.

IV. PHASOR DETECTION

The effectiveness of multifrequency phasor analysis depends on the correct identification of the set S as, in practice, phasor components must be detected from data. For ease of discussion, we consider the case where the set S is built up iteratively, progressively adding the corresponding non-zero sub-vector elements to $\underline{\mathbf{p}}$. We indicate by $\hat{\underline{\mathbf{p}}}(i)$ the estimate obtained at the i -th iteration with the index set $S(i)$. The approximation residual is $\underline{\mathbf{r}}(i) = \underline{\mathbf{x}} - \mathbf{E}_{S(i)} [\text{diag}\{\mathbf{T}\}]_{S(i)} \hat{\underline{\mathbf{p}}}(i)$.

The detection criterion to find a new frequency index is:

$$l_{i+1} = \arg \max_{0 \leq l < PN} \|\mathbf{T}^T \mathbf{E}_l^* \underline{\mathbf{r}}(i)\|_2. \quad (21)$$

Starting with an initially empty set $S(0) = \emptyset$, the index set is augmented: $S(i+1) = S(i) \cup \{l_{i+1}\}$, until the threshold ζ in (18) is reached. At each new iteration $\hat{\underline{\mathbf{p}}}(i)$ is fully recalculated, providing a refined estimate that allows to correctly take into

account possible cross-interference among phasor components, thus providing a more accurate residual vector.

Phasor detection based on (21) has a simple interpretation as the search for peaks of the estimation residual amplitude spectrum. To show this, we note that elements of vector $\underline{\mathbf{r}}(i)$ are the time-domain samples of the original signal, less the estimated contribution of the i most significant phasors. We indicate their DTFT by $R_i(\nu)$ and define: $\Delta'_\nu = \Delta'_f T_s$. From (6) and (7) it then follows:

$$\|\mathbf{T}^T \mathbf{E}_l^* \underline{\mathbf{r}}(i)\|_2 = \sqrt{\sum_{k=0}^K |T^{(k)}(\nu) \otimes R_i(\nu)|_{\nu=l\Delta'_\nu}^2}. \quad (22)$$

Since the zero-order TF coefficient is the most significant, we can adopt a simplified detection criterion, whereby the search is carried out using only the zero-order term $T^{(0)}(\nu) = D(\nu)$ in (22). Algorithm analysis can then be directly related to the properties of the Dirichlet kernel (13). An added benefit is that computation of $|D(\nu) \otimes R_i(\nu)|_{\nu=l\Delta'_\nu}$ is straightforward, through a zero-padded DFT of $\underline{\mathbf{r}}(i)$ with padding factor P .

V. MULTIFREQUENCY ANALYSIS

In this Section we focus on the ability of the CSTFM algorithm to analyze typical waveform distortion conditions, with measurement performance bounded by sensitivity rather than by interference among phasors. Although in recent measuring units the quantizer resolution can be as good as 18 bits, it would be grossly unrealistic to assume that total uncertainty remains within the least significant bit. Broadband noise summarizes as well contributions from disturbances and inaccuracies in the data acquisition system. We assume a 60 dB signal-to-noise ratio (SNR), that is an equivalent number of bits of about 10, to be a realistic representation of the rather demanding environment in an electrical distribution network.

It was shown in [11] that correct recovery of signal frequency components can be achieved by a CS-based approach when SNR > 15 dB, which leaves a useful range of 45 dB, or about two orders of magnitude as far as phasor magnitudes are concerned. In practice, sensitivity is usually good enough to allow detection of phasor components down to even less than 1% of the fundamental.

Since the cases analyzed in the next Section will be examples from the Hydro-Québec grid, for ease of comparison a nominal frequency $f_0 = 60$ Hz will be considered in numerical results throughout the paper.

A. Observation interval and frequency resolution

Frequency resolution ΔF_{min} refers, by definition, to the minimum distance at which detection of two separate, equal-magnitude, static frequency components is possible. It is inversely proportional to measurement time T_W and can be given in general as:

$$\Delta F_{min} = \frac{\kappa}{T_W}. \quad (23)$$

The constant κ is specific to the measurement algorithm. For the case considered here $\kappa \cong 1.5$ in the worst-case condition

[11], regardless of the algorithm frequency grid step size. Frequency separation between harmonic phasors is known in advance and setting $\Delta F_{min} = f_0$ gives for T_W a length of one and a half power system cycles. However it is advisable to account for the possible presence of interharmonics, at least to provide built-in robustness to spectral interference. For this purpose, the minimum distance condition must refer to harmonic-to-interharmonic distance, that will always yield $\Delta F_{min} < f_0$. Observation length needs to be increased accordingly, although long measurement intervals are less than ideal when non-stationary conditions are to be dealt with. In the following we shall consider $T_W = 100$ ms, that is, half the time suggested in [12], [13] for measurement of interharmonic groups in 5-Hz intervals. According to (23), therefore, $\Delta F_{min} = 15$ Hz.

B. Experimental results

We synthesized for this test a waveform including, in addition to the fundamental, a set of 5 harmonics (from 120 to 360 Hz) and a single interharmonic located at 90 Hz. The largest harmonic component, at 120 Hz, is 2.2% of the fundamental, others having decreasing amplitudes of 0.8%, 0.3%, 0.1% and 0.04% as the frequency increases. Interharmonic amplitude is 2% of the fundamental. These values might be considered comparatively large, though not unrealistic, at least for a current waveform. They were selected with the aim of having some limited degree of interference affecting the fundamental phasor, so that performance of the CSTFM algorithm can be more thoroughly illustrated.

We assume acquisition at the sampling rate $1/T_s = 5000$ Hz, resulting in a sequence length of 500 samples with $T_W = 100$ ms. At $f_0 = 60$ Hz this interval corresponds to six power line cycles. The plot of Fig. 1 refers to a total measurement time of 0.5-s, where sequences have been overlapped to achieve a 60-Hz reporting rate, producing a set of 30 phasor measurements. TVE values of the fundamental, interharmonic and second harmonic are reported in the figure and summarized in Table I.

The test outcome confirms that small distortion terms can be effectively detected and measured. Mean TVE $< 0.5\%$ is claimed for 90-Hz and 120-Hz components, whose magnitude is just 2% of the fundamental. It is also important to note that for the phasor at fundamental frequency mean TVE is two orders of magnitude lower than the acceptance limit set in IEEE Std. C37.118.1 [14]. As mentioned in the Introduction, several factors make TVE improvement, by at least an order of magnitude, a necessity in distribution environments. This result shows that CSTFM algorithm performance largely exceeds

TABLE I
TVE FOR HARMONIC AND INTERHARMONIC COMPONENTS

Component	Mean [%]	Std. Dev. [%]	Max [%]
60 Hz <i>fundamental</i>	0.01	0.004	0.015
90 Hz <i>interharmonic</i>	0.4	0.2	0.9
120 Hz <i>harmonic</i>	0.4	0.2	0.9

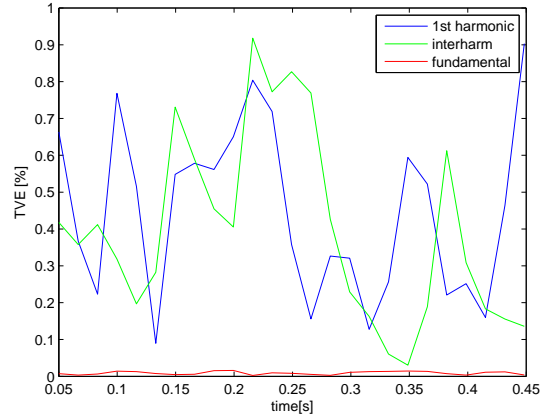


Fig. 1. TVE for 60-Hz fundamental, 90-Hz interharmonic and 120-Hz harmonic components.

the requirement, providing suitable allowance in measuring system design for the uncertainty of voltage and/or current transducers, arguably the prevailing factor in the total budget.

The test was repeated for SNR = 50 dB, which proved to be a limiting value, as far as frequency detection is concerned, for this kind of waveform.

VI. PHASOR ANALYSIS FUNCTIONS

Real-life operating conditions in some distribution networks may prove harder than test conditions considered presently in PMU characterization. To illustrate potential use of the CSTFM algorithm in a multifunction measuring unit, we consider a set of synthetic data reproducing the characteristics of some voltage waveforms in the Hydro-Québec grid, as presented in [1]. These are particularly tough trials since, due to peculiar grid operating conditions, the 60-Hz fundamental component is subject to frequency deviation and distortions well beyond the limits current in synchrophasor standards [14].

In the first test, we demonstrate the capability of CSTFM to support operation in conditions of severe distortion. The waveform under analysis, depicted in Fig. 2 and reproduced in MatLab, is modelled as a sinusoidal fundamental component with superposed harmonic and interharmonic disturbances. Fundamental amplitude is normalized to 1 p.u. with nominal frequency equal to 60 Hz. Harmonic amplitude is equal to 0.05 p.u. for 2nd- to 5th-order terms and 0.02 p.u. for orders up to 10th. Three interharmonic components are also present and their parameters are given in Table II.

TABLE II
PARAMETERS OF TEST INTERHARMONIC COMPONENTS

IH index	Parameter	Range	Selected Value
$ih = 1$	f_1	25 ÷ 32 Hz	29 Hz
	A_1	up to 25 mp.u.	25 mp.u.
$ih = 2$	f_2	70 ÷ 100 Hz	90 Hz
	A_2	up to 0.1 p.u.	0.1 p.u.
$ih = 3$	f_3	5 ÷ 20 Hz	7 Hz
	A_3	up to 0.25 p.u.	0.25 p.u.

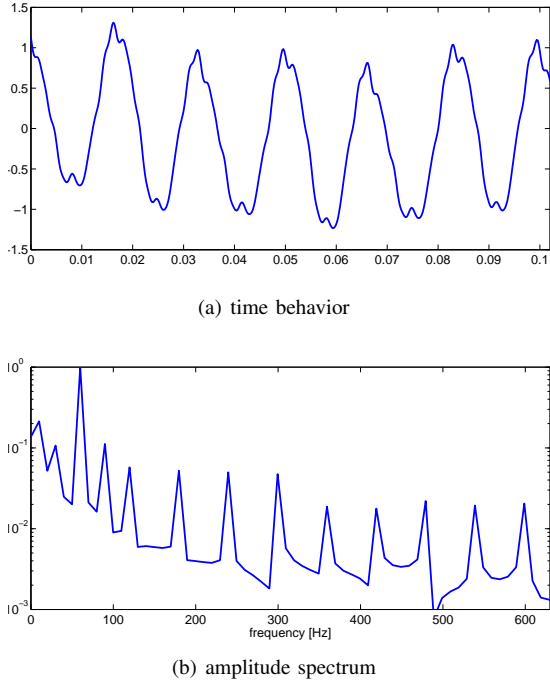


Fig. 2. Analyzed waveform with harmonic and interharmonic distortion.

Analysis of frequency separation among the fundamental, harmonic and interharmonic components evidences that $\Delta F_{min} = 14$ Hz, which is the distance between the interharmonic listed in the third line of Table II and its image. Therefore, observation interval length should be $\cong 1.5/14 = 107$ ms to meet condition (23). We again approximate this to $T_W = 100$ ms. Acquisition and reporting rate parameters are the same as before, but the assumed total test duration is now 1 s, that yields a set of 60 phasor measurements.

The CSTFM algorithm estimated TF coefficients up to order $K = 2$, using three TFM models of increasing complexity. For each of them, Table III reports the mean value, standard deviation and maximum value of TVE for the phasor at fundamental frequency only. In the first line the single-phasor estimate $\hat{p}(1)$ is employed. In the second line, the TFM model includes only harmonic components. The fact that there is very little improvement should not be surprising, as $\Delta_f = 1/T_W = 10$ Hz and the frequency separation among harmonics is equal to $6\Delta_f$, ensuring negligible interference. This is in fact reflected by the modest reduction in TVE, from 2.7% to 2.3%, achieved in this case.

Interharmonics listed on the first two lines of Table III are closer to the fundamental, at a distance of about $3\Delta_f$. In particular, since the 90-Hz component magnitude is 10%

TABLE III

FUNDAMENTAL TVE FOR DIFFERENT TFM MODEL COMPOSITION

TF Model	Mean [%]	Std. Dev. [%]	Max [%]
<i>fundamental only</i>	2.7	0.4	5.5
<i>fund. + harmonics</i>	2.3	0.4	5.1
<i>f. + h. + interharm.</i>	0.6	0.1	1.2

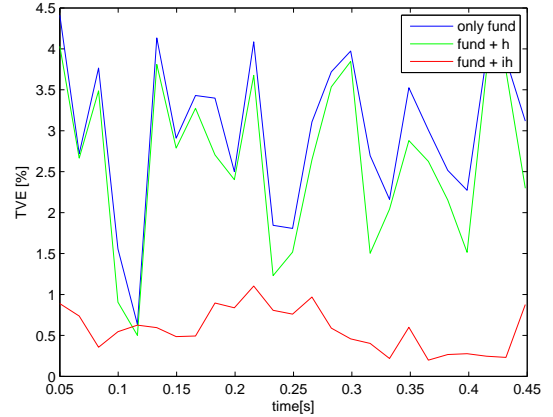


Fig. 3. TVE of phasor estimate at power line frequency for the waveform of Fig. 2. Reporting rate: 60 Hz.

of the fundamental, potential interference at the fundamental frequency is in the region of 1% of the fundamental itself. The large interharmonic at 7 Hz (25% of the fundamental, at a distance of $\cong 5\Delta_f$) can also contribute a similar amount. This assessment evidences that interharmonics are actually the main candidates for inclusion in the TFM model. Results presented in the third line of Table III prove that, although greater algorithm complexity is incurred, this allows to still meet the TVE specification in [14]. A plot of TVE values reported at 60-Hz rate over a 500 ms interval is shown in Fig. 3. In spite of the particularly demanding waveform composition, TVE usually remains within its specified limit, while measurement interval is not exceedingly long.

It is also of interest to analyze the accuracy of frequency estimates. Results for Frequency Error (FE) at the power line frequency are summarized in Table IV. Exploiting higher-order TF coefficients, estimate variability is about an order of magnitude smaller than the fine grid step Δ'_f .

TABLE IV

FREQUENCY ERROR (FE) FOR DIFFERENT TFM MODEL COMPOSITION

TF Model	Mean [Hz]	Std. Dev. [Hz]	Max [Hz]
<i>fundamental only</i>	-0.005	0.1	0.17
<i>fund. + harmonics</i>	-0.004	0.11	0.18
<i>f. + h. + interharm.</i>	-0.011	0.03	0.06

Further complexity has been added to the second trial presented here, by including waveform components associated with intermodulation phenomena, reportedly [1] due to coupling of transformers saturation and sub-synchronous parallel resonance. The test demonstrates the capability to analyze these conditions providing suitably accurate measurements.

The same waveform as before is considered and parameters of the two additional interharmonic terms are reported in Table V. Both components are exactly at the same minimum frequency separation from the fundamental given above (i.e., $\Delta F_{min} = 14$ Hz), with equal magnitudes of 5% p.u.. Consequently they generate a significant amount of interference,

TABLE V
INTERMODULATION COMPONENT PARAMETERS

IH index	Parameter	Range	Selected Value
$ih = 4$	F_4	40 ÷ 54 Hz	46 Hz
	A_4	up to 50 mp.u.	50 mp.u.
$ih = 5$	F_5	66 ÷ 80 Hz	74 Hz
	A_5	up to 50 mp.u.	50 mp.u.

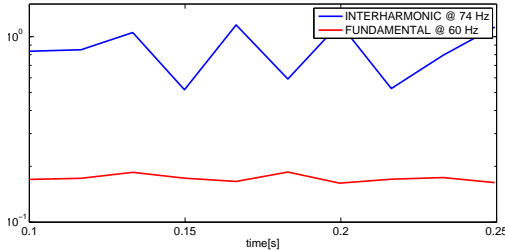


Fig. 4. TVE for 60-Hz fundamental and 74-Hz interharmonic component. Measured waveform includes the intermodulation frequencies of Table V.

but often remain undetected by (21), since the value of T_W chosen above was set at the limit of detection capability. To restore measurement accuracy, the measurement interval in this case needs to be increased to $T_W = 200$ ms (that is, the IEC 61000-4-7 measurement interval), reducing the frequency grid step Δ_f by two.

Obviously, with this waveform the full TFM model, including interharmonics, has been employed to estimate phasors. Plots of TVE for both the fundamental and the 74-Hz interharmonic component are presented in Fig. 4 for an interval of 250 ms, during which results are reported at 60-Hz rate. Corresponding TVE values are summarized in Table VI, showing again that the phasor measurement at the fundamental frequency meets the TVE specification, but also that the interharmonic phasor has been determined with comparable accuracy. Therefore analysis of intermodulation phenomena can take place while, simultaneously, the fundamental phasor is monitored.

TABLE VI
TVE FOR FUNDAMENTAL AND INTERHARMONIC COMPONENT

Component	Mean [%]	Std. Dev. [%]	Max [%]
60 Hz <i>fundamental</i>	0.17	0.003	0.2
74 Hz <i>interharmonic</i>	0.9	0.1	1.2

VII. CONCLUSIONS

Multifrequency phasor analysis is a powerful tool for measurement, analysis and monitoring in smart distribution networks, that can support as well grid-wide PQ analysis and tracking.

Depending on the purpose of the analysis, TFM-based measurement can be focused on different aspects of a waveform, providing either accurate single-phasor measurements, or comprehensive multifrequency phasor analysis with good sensitivity. Criteria have been provided to determine a minimum-

length observation interval, showing that accurate measurements of TVE and frequency can be obtained for all phasor components. At the present state of development, the algorithm is proving to be flexible and adaptable. Making the approach a truly effective proposition in terms of computing power and cost is among the challenges and future research developments.

ACKNOWLEDGMENT

This research is wholly funded by the University of Padua and is a contribution to the European Metrology Research Programme (EMRP) Joint Research Project “Smart Grids II”.

REFERENCES

- [1] I. Kamwa, S. Samantaray, and G. Joos, “Compliance analysis of PMU algorithms and devices for wide-area stabilizing control of large power systems,” *IEEE Trans. Power Syst.*, vol. 28, no. 2, pp. 1766–1778, May 2013.
- [2] D. Petri, D. Fontanelli, and D. Macii, “A frequency-domain algorithm for dynamic synchrophasor and frequency estimation,” *IEEE Trans. Instrum. Meas.*, vol. 63, no. 10, pp. 2330–2340, Oct. 2014.
- [3] P. Romano and M. Paolone, “Enhanced interpolated-DFT for synchrophasor estimation in FPGAs: Theory, implementation, and validation of a PMU prototype,” *IEEE Trans. Instrum. Meas.*, vol. 63, no. 12, pp. 2824–2836, Dec. 2014.
- [4] M. A. Platas-Garza and J. A. de la O Serna, “Dynamic harmonic analysis through Taylor-Fourier transform,” *IEEE Trans. Instrum. Meas.*, vol. 60, no. 3, pp. 804–813, Mar. 2011.
- [5] P. Castello, J. Liu, C. Muscas, P. A. Pegoraro, F. Ponci, and A. Monti, “A fast and accurate PMU algorithm for P+M class measurement of synchrophasor and frequency,” *IEEE Trans. Instrum. Meas.*, vol. 63, no. 12, pp. 2837–2845, Dec. 2014.
- [6] J. de la O Serna, “Synchrophasor measurement with polynomial phase-locked-loop Taylor-Fourier filters,” *IEEE Trans. Instrum. Meas.*, vol. 64, no. 2, pp. 328–337, Feb. 2015.
- [7] M. Bertocco, G. Frigo, C. Narduzzi, and F. Tramarin, “Resolution enhancement by compressive sensing in power quality and phasor measurement,” *IEEE Trans. Instrum. Meas.*, vol. 63, no. 10, pp. 2358–2367, Oct. 2014.
- [8] M. Bertocco, G. Frigo, C. Narduzzi, C. Muscas, and P. A. Pegoraro, “Compressive sensing of a Taylor-Fourier Multifrequency model for synchrophasor estimation,” *IEEE Trans. Instrum. Meas.*, vol. 64, no. 12, pp. 3274–3283, Dec. 2015.
- [9] J. A. de la O Serna, “Dynamic phasor estimates for power system oscillations,” *IEEE Trans. Instrum. Meas.*, vol. 56, no. 5, pp. 1648–1657, Oct. 2007.
- [10] J. Tropp and A. Gilbert, “Signal recovery from random measurements via orthogonal matching pursuit,” *Information Theory, IEEE Transactions on*, vol. 53, no. 12, pp. 4655–4666, Dec 2007.
- [11] G. Frigo and C. Narduzzi, “Compressive sensing with an overcomplete dictionary for high-resolution DFT analysis,” in *Signal Processing Conference (EUSIPCO), 2014 Proceedings of the 22nd European*, Sept 2014, pp. 1766–1770.
- [12] *Electromagnetic compatibility (EMC) – Part 4-7: Testing and measurement techniques – General guide on harmonics and interharmonics measurements and instrumentation, for power supply systems and equipment connected thereto*, International Standard IEC 61000-4-7, Aug. 2002.
- [13] A. Testa, M. Akram, R. Burch, G. Carpinelli, G. Chang, V. Dinavahi, C. Hatziaodoniu, W. Grady, E. Gunther, M. Halpin, P. Lehn, Y. Liu, R. Langella, M. Lowenstein, A. Medina, T. Ortmeier, S. Ranade, P. Ribeiro, N. Watson, J. Wikston, and W. Xu, “Interharmonics: theory and modeling,” vol. 22, no. 4, pp. 2335–2348, Oct. 2007.
- [14] *IEEE Standard for Synchrophasor Measurements for Power Systems*, IEEE Std C37.118.1-2011 (Revision of IEEE Std C37.118-2005), Dec. 2011.